Nonlinear responses of particulate nitrate to NO_x emission controls in the megalopolises of China

Mengmeng Li[1, *], Zihan Zhang[1], Tijian Wang[1], Min Xie[1], Shu Li[1], Bingliang Zhuang[1] and Yong Han[2]

[1] School of Atmospheric Sciences, Nanjing University, Nanjing 210023, China

[2] Guangdong Province Key Laboratory for Climate Change and Natural Disaster Studies, School of Atmospheric Sciences, Sun Yat-Sen University, Guangzhou, China

[*] Corresponding author: mengmengli2015@nju.edu.cn

Abstract

Nitrate is an increasingly important component of fine particulate matter ($PM_{2.5}$) in Chinese cities. The production of nitrate is not only related to the abundance of its precursor but also supported by the atmospheric photochemical oxidants, raising a new challenge to the current emission control actions in China. This paper uses comprehensive measurements and a regional meteorology-chemistry model with optimized mechanisms to establish the nonlinear responses between particulate nitrate and nitrogen oxides (NO_x) emission controls in the megalopolises of China. Nitrate is an essential component of $PM_{2.5}$ in eastern China, accounting for 9.4–15.5% and 11.5–32.1% of the $PM_{2.5}$ mass for the warm and cold seasons. The hypothetical NO_x emission reduction scenarios (−10%~−80%) during summer-autumn result in almost linearly lower $PM_{2.5}$ by −2.18% in Beijing-Tianjin-Hebei (BTH) and −2.89% in Yangtze River Delta (YRD) per 10% cut of NO_x emissions, whereas they lead to a rather complicated response of PM components in winter. Wintertime nitrate is found to increase by +4.12% in BTH and +5.05% in YRD per 10% cut of NO_x emissions, with nearly unchanged nitric acid (HNO_3) and higher dinitrogen pentoxide (N_2O_5) intermediate products produced from the increased atmospheric oxidants levels. An

inflexion point appears at 40–50% NO_x emission reduction, and a further cut in NO_x emissions is predicted to cause −10.49% reduction of nitrate for BTH and −7.68% for YRD per 10% cut of NO_x emissions. In addition, the 2012–2016 NO_x control strategy actually leads to no changes or even increases of nitrate in some areas (8.82% in BTH and 14.41% in YRD) during winter. Our results also emphasize that ammonia (NH_3) and volatile organic compounds (VOC_s) are effective in controlling nitrate pollution, whereas decreasing the sulfur dioxide (SO_2) and NO_x emissions may have counter-intuitive effects on nitrate aerosols. This paper helps understand the nonlinear aerosol and photochemistry feedbacks, and defines the effectiveness of proposed mitigations for the increasingly serious nitrate pollution in China.

1 Introduction

Secondary inorganic aerosols (SIA), including sulfate (SO_4^{2-}), nitrate (NO_3^-) and ammonium (NH_4^+) account for 30–60% of the total fine particulate matter ($PM_{2.5}$) mass during haze events in China (Huang et al., 2014a; Zhao et al., 2013). Since the enactment of the Air Pollution Action Plan in 2013, the Chinese government has taken drastic measures to reduce the emissions of sulfur dioxide (SO_2), nitrogen oxides (NO_x) and primary $PM_{2.5}$, leading to significant decreases in sulfate and overall $PM_{2.5}$ concentrations in cities (Silver et al., 2018; Li et al., 2021a; Wang et al., 2017b). Meanwhile, the nitrogen/sulfur (N/S) ratio in $PM_{2.5}$ increased significantly and nitrate had been the main component of $PM_{2.5}$ (16–45%) during haze episodes, despite a more than 20% reduction in the concentrations of its precursor NO_x (Shao et al., 2018; Wen et al., 2018; Zhai et al., 2019). The increasingly serious nitrate pollution has emerged to be the new emphasis of air pollution controls in China.

Nitrate formation involves complex multiphase chemical reactions. In the daytime, nitrogen dioxide (NO_2) reacts with hydroxyl radical (OH) to produce nitric acid (HNO_3). With excess ammonium (NH_3), low temperature and insufficient sulphuric acid, this reaction can proceed quickly and produce high ammonium nitrate (Seinfeld and Pandis, 2006). In the nighttime, however, high-concentration NO_2 reacts with ozone (O_3) to produce the nitrate radical (NO_3) and dinitrogen pentoxide (N_2O_5). The heterogeneous hydrolysis of N_2O_5 on wet particles is the main pathway for nocturnal nitrate formation (56–97%) (He et al., 2018; Pathak et al., 2011; Xue et al., 2014).

Nitrate chemistry is not only related to the abundance of its precursor NO_x, but also supported by the atmospheric oxidants (e.g., OH and O_3) produced from the photochemical reactions of NO_x and volatile organic compounds (VOC_s) (Meng et al.,

1997). Using a box model, some studies have determined that the relationship between particulate nitrate and NO_x emissions is nonlinear depending on the ozone chemical sensitivity regime (Pun and Seigneur, 2001; Nguyen and Dabdub, 2002). Pun and Seigneur (2001) showed that the daytime HNO_3 production was more sensitive to the concentrations of atmospheric oxidants, and that in the VOC-limited regime the decrease of HNO_3 production due to the NO_x emission control might be offset by the increase of OH. Nguyen and Dabdub (2002) calculated the detailed isopleth between nitrate and NO_x emissions; they found that the reduction of NO_x emissions resulted in a decrease of nitrate in the NO_x-limited regime, and an increase of nitrate under extreme conditions in the VOC-limited regime. Despite that, the single-site box model results could not distinguish the regional differences among chemical regimes; the basic hypotheses in box models to predict nitrate production are also unreasonable in the real atmosphere.

As an important precursor for both fine particles and ozone, the strict control of NO_x emissions has started in China since the 12th Five-Year Plan (Zheng et al., 2018). A confounding factor is that, for most cities in China, the production of O_3 is usually limited by VOC_s (Xie et al., 2014; Dong et al., 2014; Liu et al., 2010). The control of NO_x emissions has therefore resulted in an increase of surface O_3 concentrations in recent years (Li et al., 2021a; Li et al., 2019a; Kalsoom et al., 2021), implying complex impacts on nitrate formation. Li et al. (2021a) and Liu and Wang (2020) examined the influencing factors on the surface O_3 trends in China from 2013 to 2017 using regional chemical models. They highlighted that the control of NO_x emissions explained 11–35% of the increased O_3 due to the nonlinear NO_x-VOC_s-O_3 chemistry, and that for most regions the magnitudes could be comparable to those resulting from the meteorological influences and aerosol effects. Some simulations thought that the

NO_x emission increase in 2005–2012 resulted in an increase of nitrate by 3.4% yr^{-1} in eastern China (Geng et al., 2017; Wang et al., 2013), and the following NO_x emission control resulted in a decrease of nitrate by 3–14% (Wang et al., 2014). Recent evidence from field observations (Fu et al., 2020) and numerical simulations (Dong et al., 2014), however, suggested that the NO_x emission reduction in China could result in an increase of nitrate in winter through increased photochemical oxidants and nocturnal N_2O_5 chemistry, but a decrease in other seasons. In the next 5–10 years, SO_2 emissions might level off in China, while NO_x emissions will become stringently controlled to ensure further air quality improvements (Zheng et al., 2018). Accurately understanding the nonlinear aerosol and photochemistry feedbacks is crucial to resolve the emerging nitrate pollution and to establish reasonable air pollution control strategies in China.

To address this issue, we use comprehensive measurements and a regional meteorology-chemistry model combined with hypothetical NO_x emission scenarios to establish the nonlinear response relationships between particulate nitrate and NO_x emission controls in the megalopolises of China. The model configurations, numerical designs and observational data are presented in Sect. 2. Sect. 3 discusses the results. Finally, a summary is presented in Sect. 4.

2 Materials and Methods

2.1 Model setup and experimental designs

This study uses the Weather Research and Forecasting-Chemistry (WRF-Chem) model version 4.1 developed by Grell et al. (2002) to simulate the regional meteorology and atmospheric chemistry. The mesoscale meteorology and air quality simulations of WRF-Chem have been improved in terms of incorporating the satellite-derived land surface parameters (Li et al., 2014; Li et al., 2017), and optimizing the

SIA formation pathways enhanced by mineral aerosols (Li et al., 2019b; Huang et al., 2014b).

The modeling domain covers two main megalopolises of China and its adjacent areas—the Beijing-Tianjin-Hebei (BTH) region and the Yangtze River Delta (YRD) region (Fig. 1). The modeling framework is configured with 81×86 grid cells at 25 km horizontal resolution. The model is run with an 84-hour model cycle, with the first 12 hours discarded as spin-up time and model outputs of each model cycle to provide chemical initial conditions for the subsequent overlapping 84-hour simulation. The 6-hour, 1°×1° National Centers for Environmental Prediction Final (NCEP/FNL) analysis fields are regularly input for the model initial and lateral boundary meteorological conditions.

The model physical configurations include the YSU boundary layer scheme (Noh et al., 2003), the RRTMG radiation scheme (Iacono et al., 2008), the Noah land surface scheme (Ek et al., 2003) and the Lin microphysics scheme (Lin et al., 1983). We have updated the land cover type and vegetation data in WRF mesoscale model with the latest land surface parameters derived from Moderate Resolution Imaging Spectroradiometer (Li et al., 2014; Li et al., 2017).

The atmospheric chemistry is simulated using the Carbon Bond Mechanism version Z (CBMZ) (Zaveri and Peters, 1999) gas-phase chemistry module coupled with a four-bin sectional Model for Simulating Aerosol Interactions and Chemistry (MOSAIC) (Zaveri et al., 2008). The aqueous-phase chemistry is based on the Carnegie Mellon University (CMU) scheme including 50 species and more than 100 reactions (Fahey and Pandis, 2001). Formation of SIA in the default WRF-Chem model accounts for the gas-phases oxidation of SO_2 and NO_2, and aqueous-phase oxidation of SO_2 by hydrogen peroxide (H_2O_2) and O_3 in cloud. We have optimized

the SIA formation pathways by including the aqueous SO_2 oxidation catalyzed by mineral ions and heterogeneous uptakes of SO_2, NO_2, NO_3, N_2O_5 and HNO_3 on mineral aerosols in the MOSAIC aerosol module (Li et al., 2019b; Huang et al., 2014b).

Anthropogenic emissions are adopted from the 2016 Multi-resolution Emission Inventory for China (MEIC) and the 2010 MIX-Asia emission inventory for regions outside of mainland China developed by Tsinghua University (http://meicmodel.org). Biogenic emissions are calculated online using the Model of Emissions of Gases and Aerosols from Nature (Guenther et al., 2006).

A series of WRF-Chem simulations is designed as summarized in Table 1. In the baseline simulation (denoted as the B0 scenario), the anthropogenic emissions in China remain unchanged at the usual levels in 2016. Simulation N0 is the same as B0, but it only considers the gas-phase oxidation production of HNO_3 ($NO_2+OH \rightarrow HNO_3$) and its subsequent partitioning to the aerosol phase of nitrate in WRF-Chem. The B0 and N0 simulations are combined to distinguish the contributions of gas-phase oxidation and heterogeneous pathways (i.e., uptakes of N_2O_5, NO_3 and NO_2) for the formation of nitrate aerosols during the warm and cold seasons. A group of sensitivity scenarios (C1~C8) are designed with the perturbed anthropogenic NO_x emissions in China cut by 10%, 20%...and 80%, respectively. The differences between B0 and C1~C8 simulations are calculated to illustrate the responses of particulate pollution in China's megacities to the NO_x emission reduction scenarios. Another simulation (E1) is designed with the anthropogenic emissions of NO_x in China set to the 2012 levels to show the impacts of 2012–2016 NO_x control strategy on particulate pollution. Additionally, in order to evaluate the effectiveness of multi-pollutants cooperative controls, three series of simulations ($C_{S\text{-}N}$, $C_{N\text{-}N}$ and $C_{V\text{-}N}$) are also supplemented with

the anthropogenic emissions of SO_2, NH_3 and VOC_s in China cut by 20%, 40%...and 80%, respectively. The differences between B0 and C_N/$C_{S\text{-}N}$/$C_{N\text{-}N}$/$C_{V\text{-}N}$ simulations are calculated to illustrate the responses of nitrate pollution in China's megacities to the multi-pollutants cooperative controls.

For all simulation scenarios, two month-long periods during the Campaign on Air Pollution and Urban Meteorology in Yangtze River Delta (CAPUM-YRD)—August 15 to September 16 (Period I) and November 24 to December 26 (Period II) in 2016, are simulated to represent the warm and cold seasons, respectively (Shu et al., 2019). The complete simulation consists of thirteen 84-hour model cycles with the first 6 days as spin-up for chemistry and the remaining model outputs for analysis.

2.2 Weather and air pollutants data

Surface meteorological observations at 186 land-based automatic stations across China (Fig. 1) are collected for model meteorological validation, including hourly data of 2 m air temperature, 2 m relative humidity and 10 m wind speed. These data are archived at the U. S. National Climatic Data Center (NCDC) (Smith et al., 2011).

Air pollutants data at the national air quality monitoring network and regional supersites of China (Fig. 1) are used for model chemical validation. This nationwide monitoring network contains 1597 sites covering 454 cities in mainland China, as shown in Fig. 1. Six routine air pollutants including $PM_{2.5}$, particulate matter with aerodynamic diameter less than 10 μm (PM_{10}), SO_2, NO_2, carbon monoxide (CO) and O_3 are monitored and reported hourly by Chinese National Environmental Monitoring Center (CNEMC) network (available at http://websearch.mep.gov.cn/).

Additionally, four comprehensive atmospheric environment supersites in YRD including Dianshanhu (DSH; 31.1ºN, 121.0°E), Pudong (PD; 31.2º N, 121.5°E), Nanjing (NJ; 32.1ºN, 118.8°E) and Hangzhou (HZ; 30.3ºN, 120.2°E) measured the

mass concentrations of $PM_{2.5}$, water-soluble ions (sulfate, nitrate, ammonium, sodium, chloride, potassium, calcium and magnesium), carbonaceous aerosols (elemental carbon (EC) and organic carbon (OC)) and gaseous pollutants (SO_2, NO_2, CO and O_3) during the CAPUM-YRD campaign. Details for the methods and data at the four supersites are described in Shu et al. (2019).

3 Results and discussions

3.1 Model weather and chemical validation

Model evaluations indicate that the WRF-Chem model is able to simulate the weather and atmospheric pollution characteristics in China. The simulated magnitudes of surface temperature by WRF-Chem in general agree with actual observations, with a correlation efficient (*R*) of 0.89 and 0.94, and a normalized mean bias (NMB) of −0.55% and −0.80% respectively in Period I and Period II (Table 2). Underestimation of relative humidity (−5.65% in Period I and −6.56% in Period II) is common in the WRF simulation and it might be attributed to the influence of the boundary layer parameterization on the weather forecast (Bhati and Mohan, 2018; Gomez-Navarro et al., 2015). Clear overestimation of wind speed (23.72% in Period I and 40.64% in Period II) might be because of the unresolved topography in WRF (Jimenez et al., 2013; Li et al., 2014).

The predicted concentrations of routine air pollutants also faithfully capture the spatial and seasonal patterns of observed surface $PM_{2.5}$, SO_2, NO_2 and O_3 levels in both seasons (Fig. 2). Both simulations and observations display high air pollutants concentrations in the vicinity of North China Plain (NCP) and eastern China, but with higher O_3 levels in the warm season and oppositely higher $PM_{2.5}$ and other gaseous pollutants concentrations in winter. The model statistical evaluations show a mean bias (MB) of −3.66, −1.14, 4.7 and 18.32 μg m^{-3}, and NMB of −9.92, −6.46, 16.47

and 7.72% for $PM_{2.5}$, SO_2, NO_2 and O_3 in Period I, and a relatively larger MB of −27.31, −11.65, 1.27 and −39.01 μg m^{-3}, and NMB of −29.82, −28.11, 2.40 and −31.05% in Period II, respectively (Table 3). The uncertainty in emissions data, the absence of secondary organic aerosol in MOSAIC aerosol chemistry or the simulated wind errors (Table 2) may be responsible for the larger atmospheric chemical biases in winter, which has been extensively discussed in some studies (Zhao et al., 2016; Li et al., 2021a).

As the most important components of $PM_{2.5}$, reasonable representation of SIA is imperative to $PM_{2.5}$ simulation. Evaluations with measurements of $PM_{2.5}$ components at the four supersites of eastern China show that the model performs reasonably in simulating the seasonal variations and proportions of aerosol species in $PM_{2.5}$, but it is biased low by 10–40% in simulating the magnitudes of SIA concentrations (Fig. 3). The model underestimation is −1.8, −2.2 and −2.2 μg m^{-3} for sulfate, nitrate and ammonium, respectively, in Period I, and −2.6, −4.3 and −3.4 μg m^{-3} in Period II. The model also captures the large change of N/S ratio from the warm to cold seasons, that increases from 0.42 in Period I to 1.56 in Period II. Our previous work (Li et al., 2019) has confirmed that the consideration of the optimized aqueous and heterogeneous SIA formation pathways in WRF-Chem significantly reduces the model biases by 41.38% for sulfate and 44.55% for nitrate during the CAPUM-YRD campaign of 2016. Recent studies highlighted that the remaining SIA simulation biases may be attributed to the missing aqueous oxidation of SO_2 by NO_2 on alkaline aerosols under humid conditions (Wang et al., 2016; Cheng et al., 2016).

3.2 Air pollution and aerosol composition characteristics

Chemical composition analyses of major gaseous and particulate air pollutants suggest large seasonal variations of air pollution characteristics in China (Fig. 2).

Mainly emitted from combustion sources, atmospheric pollutants accumulate in the densely industrialized and populated megalopolises of China, with a hotspot along Beijing, Hebei, Shandong and their adjacent cities frequently exceeding China's National Ambient Air Quality Standards. The average concentrations of surface $PM_{2.5}$, SO_2, NO_2 and daily-maximum O_3 in China's routine air quality monitoring network are 36.88, 17.65, 28.53 and 237.45 μg m^{-3} for Period I, and 91.59, 41.45, 53.01 and 125.62 μg m^{-3} for Period II. The surface $PM_{2.5}$, SO_2 and NO_2 concentrations show obvious increases by 148.35%, 134.84% and 85.80% during winter compared to those of the summer-autumn period (Period I). The maximum surface $PM_{2.5}$ concentrations recorded in the winter period was more than 600 μg m^{-3}, which is the highest value ever recorded in 2016 and leads to the "orange" air quality alert.

The further analyses of $PM_{2.5}$ mass concentrations, major $PM_{2.5}$ components and gases at the four supersites in YRD are presented in Fig. 4–5. Organic matter (OM) is obtained by multiplying the OC concentrations by a factor of 1.6, mainly accounting for the hydrogen and oxygen masses in OM. The measured SIA concentrations exhibit high levels, with average values of 18.8 μg m^{-3} for Period I and 37.1 μg m^{-3} for Period II. The three SIA components together account for 32.3–57.4% (48.6% on average) and 27.7–70.9% (56.9% on average) of the total $PM_{2.5}$ mass concentrations, and become the primary components of $PM_{2.5}$ in the two periods. The proportions of sulfate, nitrate and ammonium in total $PM_{2.5}$ range from 13.5–28.9%, 9.4–15.5% and 9.4–14.9% at the four supersites for Period I, and 9.2–20.3%, 11.5–32.1% and 7.0–19.8% for Period II, respectively. The strikingly higher proportion of nitrate than that of sulfate in $PM_{2.5}$ during winter, with a N/S ratio of 1.56, is in accordance with recent observations during other winter haze periods in China (Shao et al., 2018; Zhang et al., 2018; Zhang et al., 2019). They emphasized that since the enactment of Clean Air

Action Plan in 2013, the $PM_{2.5}$ components had changed clearly with decreasing contributions from coal combustion.

The high proportions of sulfate and nitrate in $PM_{2.5}$ could be related to the high oxidation rates of SO_2 and NO_2. The observed average values of sulfur oxidation ratio ($SOR=[SO_4^{2-}]/([SO_4^{2-}]+[SO_2])$) and nitrogen oxidation ratio ($NOR=[NO_3^-]/([NO_3^-]+[NO_2])$) are 0.41 and 0.13 in Period I, and 0.33 and 0.21 in Period II. In contrast, the observed SOR is generally higher in summer-autumn than winter, opposite to that of NOR, indicating the enhanced formation of nitrate in winter. Shu et al. (2019) also noted similar seasonal distinctions for SOR and NOR in YRD. They attributed the weakened conversion from NO_2 to nitrate in summer to the volatility and evaporative loss of nitrate (Sun et al., 2012). The sharp increase of particles and moderate ambient humidity in winter also benefit the heterogeneous formation of SIA, leading to high NOR and SOR (Wang et al., 2012).

Figure 6 illustrates the contributions of gas-phase oxidation and heterogeneous reactions for the nitrate production calculated from B0 and E0 simulations. It is shown that on a daily basis the gas-phase oxidation production of HNO_3 and its subsequent partitioning to the aerosol phase is the principal formation route for particulate nitrate, with the average contributions of 60.19% for BTH and 91.71% for YRD in Period I and 75.14% for BTH and 85.94% for YRD in Period II. The heterogeneous hydrolyses of N_2O_5 and other nitrogenous gases (calculated as the model differences between B0 and N0 simulations) contribute to the remaining nitrate, particularly in BTH with high aerosol loading. These calculated results (60.19–91.71% for NO_2+OH oxidation and 8.29–39.81% for heterogeneous pathways) are in line with previous assessments in China and globally. Alexander et al. (2009) reported that the global tropospheric nitrate burden is dominated by NO_2+OH (76%), followed by N_2O_5

hydrolysis (18%); but recent results suggested that N_2O_5 hydrolysis was as important as $NO_2 + OH$ (both 41 %) for global nitrate production (Alexander et al., 2020). In major Chinese cities, it was estimated that the conversion of NO_x to nitrate was dominated by NO_2 +OH oxidation in Shanghai, with a mean contribution of 55–77% in total and even higher (84–92%) in summer (He et al., 2020). In NCP, the nitrate contribution of heterogeneous pathways was about 30.8% (Liu et al., 2020) or even comparable to the partitioning of HNO_3 (Wang et al., 2019; Wang et al., 2017a; Luo et al., 2021). The nitrate formation from heterogeneous pathways is moderately underestimated in the optimized WRF-Chem model of this study, possibly due to the uncertainties of heterogeneous uptake coefficients and unclear reaction mechanisms applied in the model (Li et al., 2019b; Xue et al., 2016; He et al., 2014).

3.3 Nonlinear responses of nitrate to NO_x emissions and their policy implications

3.3.1 $PM_{2.5}$-NO_x and O_3-NO_x responses in the warm and cold seasons

NO_x is key in atmospheric chemistry and serves as an important precursor for both ozone and secondary aerosols. We conduct a series of simulations (C1~C8) with perturbed NO_x emissions to assess the responses of $PM_{2.5}$ mass concentrations to NO_x emissions in two megalopolises of China (Fig. 7). The WRF-Chem simulation results show that the responses of surface $PM_{2.5}$ concentrations to NO_x emissions vary in different seasons and display strong nonlinear behaviour in winter. To better quantify their effectiveness, we define the NO_x emission control efficiency (β), which denotes the percentage changes of surface $PM_{2.5}$ or its components concentrations in response to the successive 10% cut of NO_x emissions.

In Period I (Aug–Sep), the $PM_{2.5}$-NO_x responses are closer to a linear function, reflecting a stronger sensitivity to the NO_x emission changes in the warm season. The surface $PM_{2.5}$ concentrations decrease almost linearly as we gradually reduce NO_x

emissions in China, with the average β values of −2.18% in BTH and −2.89% in YRD. However, the $PM_{2.5}$-NO_x emission responses in Period II (Nov–Dec) display strong nonlinearity and are analogous to a quadratic parabola distribution for both regions. The NO_x emission reductions within the first 50% would even increase surface $PM_{2.5}$ concentrations by +1.25% averagely in BTH, and this β value increases to +1.76% in YRD with the first 40% reductions of NO_x emissions. Subsequently, the $PM_{2.5}$ responses shift towards a similar linear pattern, with an average β value of −2.51% in BTH and −3.96% in YRD.

The distinct forms of $PM_{2.5}$-NO_x emission responses for the warm and cold seasons are determined by the seasonal ozone chemical sensitivity regimes. The photochemical indicator of $\Delta[O_3]_{NOx}/\Delta[O_3]_{VOCs}$ with a critical value of 1.0 is used to investigate the season-varying ozone sensitivity in China, which is calculated as the ratio of ozone concentration changes under 20% NO_x emission reduction to that under 20% VOC_s emission reduction (Fig. S1). The results indicate a strong VOC-limited ozone chemistry across China during winter, while either VOC-limited regime over a large portion of NCP and eastern China or NO_x-limited regime in northern and western China during summer-autumn, as also indicated from previous studies (Xie et al., 2014; Dong et al., 2014; Liu et al., 2010). We find larger O_3 and OH productions under the NO_x emission reduction conditions in both seasons (Fig. 8–9), particularly in Period II (Nov–Dec) with an average increase rate of +14.72% and +18.50% in BTH and +25.17% and +23.09% in YRD per 10% cut of NO_x emissions. The SIA formation chemistry is highly limited by atmospheric oxidants produced from the NO_x-VOC_s-O_3 photochemical cycles. The nonlinear O_3-NO_x responses indicate a rather complicated aerosol and photochemistry feedback in megacities.

3.3.2 Nonlinear responses of particulate nitrate to NO_x emissions

The SIA formation is basically driven by the atmospheric oxidants levels, and a reduction of NO_x emissions may have counter-intuitive effects on SIA components by controlling the atmospheric oxidants levels. The calculated SIA components for each emission scenario in both months show that the surface nitrate aerosols can be substantially decreased/increased with reducing NO_x emissions, but the sulfate and ammonium concentrations have moderately smaller changes (Fig. 8–10).

Response of sulfate to the NO_x emissions is more predictable and determined by the changes of atmospheric oxidants levels since that the conversion of SO_2 to sulfate is partly driven by OH in the gas-phase and by dissolved H_2O_2 or O_3 in the presence of fog or cloud. In Period I (Aug–Sep), the sulfate-NO_x response follows a gradual quadratic parabola distribution as that of O_3-NO_x and OH-NO_x response curves (Fig. 8 and Fig. 10), with a fitted function in Eq. 1. The β values for surface sulfate change by −0.74%~+1.16% in BTH and −1.54%~+0.17% in YRD under the −10~−80% NO_x emission reduction scenarios.

$$[SO_4^{2-}]=-2.45\Delta E_{NOx}^2-2.15\Delta E_{NOx}+5.90 \text{ in BTH} \quad (R^2=0.9309) \qquad \text{(Eq. 1)}$$

$$[SO_4^{2-}]=-2.26\Delta E_{NOx}^2-1.31\Delta E_{NOx}+6.65 \text{ in YRD} \quad (R^2=0.9893)$$

where $[SO_4^{2-}]$ is the surface mean concentration of sulfate (μg m^{-3}); ΔE_{NOx} is the percentage change of NO_x emissions (%).

As expected, the production of nitrate reflects a strong sensitivity to NO_x and it decreases linearly with the NO_x emission control, with an average β value of −10.21% in BTH and −11.51% in YRD, which further leads to a decrease of ammonium concentrations by −3.25% in BTH and −4.35% in YRD (Fig. 8 and Fig. 10). The formation of nitrate mainly involves the $NO_2+OH\rightarrow HNO_3$ gas-phase oxidation and the heterogeneous hydrolysis of N_2O_5 and other nitrogenous gases. The strong

sensibility of particulate nitrate in response to the NO_x emission decreases can be explained by the synchronously suppressive production of its intermediate products HNO_3 and N_2O_5. For example, when the NO_x emission is cut by 20%, the surface NO_2 concentration in BTH drops by 21.96% but the surface O_3 and OH concentrations increase slightly by 2.56% and 5.28% due to the reduction of $NO+O_3$ titration reaction and the greater VOC availability in the warm season, leading to substantial reductions in surface HNO_3 (−16.72%) and N_2O_5 (−8.94%) concentrations.

$$[NO_3^-] = -34.54\Delta E_{NOx}^2 - 30.66\Delta E_{NOx} + 10.52 \text{ in BTH} \quad (R^2=0.8379) \quad \text{(Eq. 2)}$$

$$[NO_3^-] = -36.53\Delta E_{NOx}^2 - 26.94\Delta E_{NOx} + 9.70 \text{ in YRD} \quad (R^2=0.9862)$$

$$[NH_4^+] = -9.12\Delta E_{NOx}^2 - 8.73\Delta E_{NOx} + 5.40 \text{ in BTH} \quad (R^2=0.7759) \quad \text{(Eq. 3)}$$

$$[NH_4^+] = -10.55\Delta E_{NOx}^2 - 8.36\Delta E_{NOx} + 4.58 \text{ in YRD} \quad (R^2=0.9762)$$

where $[NO_3^-]$ and $[NH_4^+]$ are the surface mean concentrations (μg m^{-3}) of nitrate and ammonium, respectively.

In Period II (Nov–Dec), we find opposite results with quadratic parabola distributions for nitrate-NO_x response (Eq. 2) and ammonium-NO_x response (Eq. 3), but linearly increasing sulfate concentrations (average β values of +2.00% in BTH and +2.64% in YRD; Fig. 9 and Fig. 10), leading to small $PM_{2.5}$ changes in winter. Such nonlinear nitrate-NO_x responses can be explained by the substantially increased oxidants as we gradually reduce NO_x emissions in each scenario. It is noted that in winter the nitrate-NO_x response highly depends on the production of N_2O_5, which is produced from the $NO_2 \xrightarrow{O_3} NO_3 \xrightarrow{NO_2} N_2O_5$ chemical reactions and is a crucial intermediate product for nitrate formation. Under the low NO_x emission reduction conditions, the production of N_2O_5 is more sensitive to the atmospheric oxidants concentrations. The significant increases of surface O_3 in each NO_x emission scenario in the VOC-poor

environment (Fig. 9(b, d)) lead to an enhancement of N_2O_5 levels from 10% to more than 100%. In spite of the HNO_3 concentration remaining nearly unchanged or decreasing slightly by less than 5% in response to NO_x control, nitrate is found to increase (average β values of +4.12% in BTH and +5.05% in YRD) with higher N_2O_5 produced from the increased ozone introduced by attenuated titration. An inflexion point appears at the 40–50% NO_x emission reduction scenario, and a further reduction in NO_x emissions is predicted to cause −10.49% and −5.31% reductions of surface particulate nitrate and ammonium for BTH, and −7.68% and −7.36% for YRD.

These results reveal that the increase in atmospheric oxidants in response to NO_x emission control can offset the decreasing precursors concentrations and further enhance the formation of secondary nitrate, as recently found during the COVID-19 pandemic (Huang et al., 2020; Li et al., 2021b).

3.3.3 Impacts of 2012–2016 NO_x control strategy on particulate pollution

During the 12th Five-Year Plan period (2011–2015), a series of end-of-pipe pollutant controls (e.g., Selective Catalytic Reduction techniques) were carried out for power, industry and transportation sectors. These measures effectively controlled the national NO_x emissions by 22.8% from 2012 to 2016 (MEIC v1.3) in China. To quantify the effects of recent NO_x control measures on the levels of photochemical oxidants and particulate nitrate, we conduct an additional simulation with NO_x emissions set to the levels of 2012 in E1.

The model simulations (Fig. 11) suggest that reducing China's NO_x emissions alone from 2012 to 2016 leads to an average −24.93%~−8.62% decrease of NO_x concentrations in the surface layer. As previously pointed out, the 2012–2016 NO_x emission control measures lead to increased O_3 and OH levels in winter, which offset the effectiveness of NO_x emission reduction in alleviating winter nitrate. No obvious

declines in the winter nitrate levels are observed and even increases in some areas (+8.82% in BTH and 14.41% in YRD; Fig. S2–S3). As shown, the largest $PM_{2.5}$ responses shift towards the southern Hebei and central China provinces, where the wintertime $PM_{2.5}$ concentrations are particularly high in this region. The substantial emission changes from 2012 to 2016 lower the $PM_{2.5}$ air pollution by up to −1.84% in BTH and −3.52% in YRD for Period I and oppositely increase the surface $PM_{2.5}$ by 2.36% in BTH and 4.67% in YRD for Period II. The past NO_x emission control strategy leads to increased atmospheric oxidants levels and deteriorated particulate pollution in winter due to the nonlinear photochemistry and aerosol chemical feedbacks, without regard to the other emission control measures. This conclusion is also supported by evidence from the recent field observations (Fu et al., 2020).

3.3.4 Responses of particulate nitrate to multi-pollutants cooperative controls

In order to evaluate the effectiveness of multi-pollutants cooperative controls in China, three series of additional simulations ($C_{S\text{-}N}$, $C_{N\text{-}N}$ and $C_{V\text{-}N}$) are also designed to show the responses of nitrate and $PM_{2.5}$ pollution to the emission controls of NO_x, SO_2, NH_3 and VOC_s, respectively. The results (Fig. 12) show that atmospheric NH_3 and VOC_s are effective in controlling the particulate nitrate pollution for both seasons, whereas decreasing the SO_2 and NO_x emissions may have counter-intuitive effects on the concentration levels of nitrate aerosols.

Atmospheric NH_3 acts as a critical neutralizing species for SIA production and efficient haze mitigation (Liu et al., 2019). According to the WRF-Chem simulation, reduction of NH_3 emissions may be effective in reducing the nitrate component, with an average β value of −9.96% in BTH and −10.35% in YRD for Period I, and −8.32% in BTH and −11.47% in YRD for Period II, primarily by suppressing the ammonium nitrate formation. Quantitatively, a 10% reduction in NH_3 emissions can alleviate the

435 $PM_{2.5}$ pollution by −2.67% during summer-autumn and −3.21% during winter in the
436 two Chinese megacities. Atmospheric chemistry modeling by Wen et al. (2021) also
437 indicated that controlling NH_3 emissions in Beijing would significantly reduce the
438 population-weighted $PM_{2.5}$ concentrations by 6.2–21% with 60–100% NH_3 reductions
439 in January, implying the need to consider NH_3 emission controls when designing the
440 $PM_{2.5}$ pollution mitigation strategies.

441 VOC_s, which is not a direct precursor for SIA, is effective in SIA controls due to
442 their influences on the atmospheric oxidation cycles (Tsimpidi et al., 2008; Womack
443 et al., 2019; Nguyen and Dabdub, 2002). Our results suggest that decreasing VOC_s
444 emissions per 10% would suppress the oxidation formation of nitrate and decrease the
445 nitrate concentrations by −2.48% in BTH and −1.69% in YRD for Period I, and
446 −5.01% in BTH and −6.35% in YRD for Period II. The reduction of VOC_s emissions
447 would result in a decrease of $PM_{2.5}$ by −0.70% during summer-autumn and −1.76%
448 during winter in the two megacities. Tsimpidi et al. (2008) also showed that the
449 reduction of VOC_s emissions caused a marginal increase of $PM_{2.5}$ during summer in
450 eastern United States, whereas it resulted in a decrease of atmospheric oxidant levels
451 and 5–20% reduction of both inorganic and organic $PM_{2.5}$ components during winter.
452 Larger and synchronized NO_x and VOC_s emissions controls are required to overcome
453 the adverse effects of nonlinear photochemistry and aerosol chemical feedbacks.

454 The SO_2 emission reduction, although effective in reducing sulfate and $PM_{2.5}$, is
455 not successful in regulating the nitrate pollution due to the chemical competition in
456 nitrate and sulfate formations (Geng et al., 2017; Wang et al., 2013). Changes in
457 nitrate concentration are linearly associated with the SO_2 emission reductions, with
458 the average β values of 2.90% during summer-autumn and 1.35% during winter.
459 Decreasing SO_2 emissions is less effective (a β value of −0.74%) in mitigating the

wintertime haze pollution because that the benefit of SO_2 reduction is partly offset by the significant increase of nitrate, demonstrating the critical role of multi-pollutants cooperative controls. Lei et al. (2013) evaluated the impacts of SO_2 control strategies on nitrate and sulfate production in USA and also found that the competition for bases in nitrate and sulfate formation significantly affects the nitrate concentrations.

Our results emphasize that future nitrate and $PM_{2.5}$ pollution mitigation strategies should focus on reducing the chemical precursors and key atmospheric oxidants involved in the production of secondary aerosols. The recent "Three-year Action Plan Fighting for a Blue Sky" calls for stringent emissions controls of NO_x, SO_2, VOC_s and NH_3 but without specific reduction targets. Such emission changes would emphasize the need to jointly consider multi-pollutants emissions controls for mitigating haze air pollution.

4 Conclusions

Recent air pollution actions have significantly lowered the $PM_{2.5}$ levels in China via controlling emissions of SO_2 and NO_x, but raised a new question of how effective the NO_x emission controls can be on the mitigation of emerging nitrate and ozone air pollution. We use comprehensive measurements and a regional meteorology-chemistry model with optimized mechanisms to establish the nonlinear responses between particulate nitrate and NO_x emission controls in the megalopolises of China.

Nitrate is an essential component of $PM_{2.5}$ in eastern China, accounting for 9.4–15.5% and 11.5–32.1% of the total $PM_{2.5}$ mass for the warm and cold seasons, respectively. We find that the efficiency of $PM_{2.5}$ reduction is highly sensitive to NO_x emissions and it varies in different seasons depending on the ozone chemical regimes. The reduction of NO_x emissions results in almost linearly lower $PM_{2.5}$ by −2.18% in BTH and −2.89% in YRD per 10% cut of NO_x emissions during summer-autumn,

whereas it increases the atmospheric oxidants levels and leads to a rather complicated response of the PM components in winter. Nitrate is found to increase (average β values of +4.12% in BTH and +5.05% in YRD) in winter with higher N_2O_5 intermediate produced from the increased ozone introduced by attenuated titration, despite the nearly unchanged or slightly decreased HNO_3 concentrations in response to NO_x control. An inflexion point appears at 40–50% NO_x emission reduction, and a further reduction of NO_x emissions is predicted to cause −10.49% reductions of particulate nitrate for BTH and −7.68% for YRD. In addition, the 2012–2016 NO_x emission control strategy leads to −24.93%~−8.62% decreases of surface NO_x concentrations, and no changes or even increases of wintertime nitrate in BTH (+8.82%) and YRD (14.41%). Our results also emphasize that atmospheric NH_3 and VOC_s are effective in controlling the particulate nitrate pollution, whereas decreasing the SO_2 and NO_x emissions may have counter-intuitive effects on nitrate aerosols. These results provide insights for developing mitigation strategies for the ubiquitous nitrate aerosols in winter haze of China.

Author contribution

Mengmeng Li developed the model code, designed the numerical experiments, and wrote the original draft. Zihan Zhang carried out the numerical experiments. Min Xie, Shu Li and Bingliang Zhuang validated and analyzed the model results. Tijian Wang and Yong Han reviewed and revised the manuscript.

Competing interests

The authors declare that they have no conflict of interest.

Acknowledgement

This study is funded by the National Natural Science Foundation of China (41975153, 42077192 and 41775056), the National Key Basic Research Development

Program of China (2019YFC0214603, 2020YFA0607802), and the Emory University-Nanjing University Collaborative Research Grant.

Data availability statement

The WRF-Chem model version 4.1 is available at http://www2.mmm.ucar.edu/wrf/users/downloads.html. The NCEP FNL data are accessible at the National Center for Atmospheric Research (NCAR) Research Data Archive (RDA; http://rda.ucar.edu/datasets/ds083.2/). The MEIC anthropogenic emission inventories are available at www.meicmodel.org, and for more information, please contact Q. Zhang (qiangzhang@tsinghua.edu.cn). The surface weather data are accessible at the Integrated Surface Database (https://www.ncdc.noaa.gov/isd/data-access). The surface air pollutants and aerosol species data are provided by Chinese National Environmental Monitoring Center (http://www.cnemc.cn/en/) and archived at https://doi.org/10.6084/m9.figshare.12818807.v1.

References

Alexander, B., Hastings, M. G., Allman, D. J., Dachs, J., Thornton, J. A., and Kunasek, S. A.: Quantifying atmospheric nitrate formation pathways based on a global model of the oxygen isotopic composition (delta O-17) of atmospheric nitrate, Atmos Chem Phys, 9, 5043-5056, 2009.

Alexander, B., Sherwen, T., Holmes, C. D., Fisher, J. A., Chen, Q. J., Evans, M. J., and Kasibhatla, P.: Global inorganic nitrate production mechanisms: comparison of a global model with nitrate isotope observations, Atmos Chem Phys, 20, 3859-3877, 2020.

Bhati, S. and Mohan, M.: WRF-urban canopy model evaluation for the assessment of heat island and thermal comfort over an urban airshed in India under varying land use/land cover conditions, Geosci Lett, 5, doi: 10.1186/s40562-018-0126-7, 2018.

Cheng, Y. F., Zheng, G. J., Wei, C., Mu, Q., Zheng, B., Wang, Z. B., Gao, M., Zhang, Q., He, K. B., Carmichael, G., Poschl, U., and Su, H.: Reactive nitrogen chemistry in aerosol water as a source of sulfate during haze events in China, Sci Adv, 2, e1601530, doi: 10.1126/sciadv.1601530, 2016.

Dong, X. Y., Li, J., Fu, J. S., Gao, Y., Huang, K., and Zhuang, G. S.: Inorganic aerosols responses to emission changes in Yangtze River Delta, China, Sci Total Environ, 481, 522-532, 2014.

Ek, M. B., Mitchell, K. E., Lin, Y., Rogers, E., Grunmann, P., Koren, V., Gayno, G., and Tarpley, J. D.: Implementation of Noah land surface model advances in the National Centers for Environmental Prediction operational mesoscale Eta model, J Geophys Res-Atmos, 108, 8851, doi: 10.1029/2002jd003296, 2003.

Fahey, K. M. and Pandis, S. N.: Optimizing model performance: variable size resolution in cloud chemistry modeling, Atmos Environ, 35, 4471-4478, 2001.

Fu, X., Wang, T., Gao, J., Wang, P., Liu, Y. M., Wang, S. X., Zhao, B., and Xue, L. K.: Persistent Heavy Winter Nitrate Pollution Driven by Increased Photochemical Oxidants in Northern China, Environ Sci Technol, 54, 3881-3889, 2020.

Geng, G. N., Zhang, Q., Tong, D., Li, M., Zheng, Y. X., Wang, S. W., and He, K. B.: Chemical composition of ambient $PM_{2.5}$ over China and relationship to precursor emissions during 2005-2012, Atmos Chem Phys, 17, 9187-9203, 2017.

Gomez-Navarro, J. J., Raible, C. C., and Dierer, S.: Sensitivity of the WRF model to PBL parametrisations and nesting techniques: evaluation of wind storms over complex terrain, Geosci Model Dev, 8, 3349-3363, 2015.

Grell, G. A., McKeen, S., Michalakes, J., Bao, J. W., Trainer, M., and Hsie, E. Y.: Real-time simultaneous prediction of air pollution and weather during the Houston 2000 field experiment, Fourth Conference on Atmospheric Chemistry: Urban, Regional And Global Scale Impacts Of Air Pollutants, 224-227, 2002.

Guenther, A., Karl, T., Harley, P., Wiedinmyer, C., Palmer, P. I., and Geron, C.: Estimates of global terrestrial isoprene emissions using MEGAN (Model of Emissions of Gases and Aerosols from Nature), Atmos Chem Phys, 6, 3181-3210, 2006.

He, H., Wang, Y. S., Ma, Q. X., Ma, J. Z., Chu, B. W., Ji, D. S., Tang, G. Q., Liu, C., Zhang, H. X., and Hao, J. M.: Mineral dust and NOx promote the conversion of SO2 to sulfate in heavy pollution days, Scientific Reports, 4, 4172, doi: 10.1038/Srep04172, 2014.

He, P. Z., Xie, Z. Q., Yu, X. W., Wang, L. Q., Kang, H., and Yue, F. G.: The observation of isotopic compositions of atmospheric nitrate in Shanghai China and its implication for reactive nitrogen chemistry, Sci Total Environ, 714, 136727, doi: 10.1016/j.scitotenv.2020.136727, 2020.

He, P. Z., Xie, Z. Q., Chi, X. Y., Yu, X. W., Fan, S. D., Kang, H., Liu, C., and Zhan, H. C.: Atmospheric Delta O-17(NO3-) reveals nocturnal chemistry dominates nitrate production in Beijing haze, Atmos Chem Phys, 18, 14465-14476, 2018.

Huang, R. J., Zhang, Y. L., Bozzetti, C., Ho, K. F., Cao, J. J., Han, Y. M., Daellenbach, K. R., Slowik, J. G., Platt, S. M., Canonaco, F., Zotter, P., Wolf, R., Pieber, S. M., Bruns, E. A., Crippa, M., Ciarelli, G., Piazzalunga, A., Schwikowski, M., Abbaszade, G., Schnelle-Kreis, J., Zimmermann, R., An, Z. S., Szidat, S., Baltensperger, U., El Haddad, I., and Prevot, A. S. H.: High secondary aerosol contribution to particulate pollution during haze events in China, Nature, 514, 218-2222014a.

Huang, X., Song, Y., Zhao, C., Li, M. M., Zhu, T., Zhang, Q., and Zhang, X. Y.: Pathways of sulfate enhancement by natural and anthropogenic mineral aerosols in China, J Geophys Res-Atmos, 119, 14165-14179, 2014b.

Huang, X., Ding, A., Gao, J., Zheng, B., Zhou, D., Qi, X., Tang, R., Wang, J., Ren, C., Nie, W., Chi, X., Xu, Z., Chen, L., Li, Y., Che, F., Pang, N., Wang, H., Tong, D., Qin, W., Cheng, W., Liu, W., Fu, Q., Liu, B., Chai, F., Davis, S., Zhang, Q., and He, K.: Enhanced secondary pollution offset reductioin of primary emissions during COVID-19 lockdown in China, Natl Sci Rev, 1-9, 2020.

Iacono, M. J., Delamere, J. S., Mlawer, E. J., Shephard, M. W., Clough, S. A., and Collins, W. D.: Radiative forcing by long-lived greenhouse gases: Calculations with the AER radiative transfer models, J Geophys Res-Atmos, 113, D13103, doi: 10.1029/2008jd009944, 2008.

Jimenez, P. A., Dudhia, J., Gonzalez-Rouco, J. F., Montavez, J. P., Garcia-Bustamante, E., Navarro, J., de Arellano, J. V. G., and Munoz-Roldan, A.: An evaluation of WRF's ability to reproduce the surface wind over complex terrain based on typical circulation patterns, J Geophys Res-Atmos, 118, 7651-7669, 2013.

Kalsoom, U., Wang, T. J., Ma, C. Q., Shu, L., Huang, C. W., and Gao, L. B.: Quadrennial variability and trends of surface ozone across China during 2015-2018: A regional approach, Atmos Environ, 245, 117989, doi: 10.1016/j.atmosenv.2020.117989, 2021.

Lei, H., Wuebbles, D. J.: Chemical competition in nitrate and sulfate formations and its effect on air quality, Atmos Environ, 80, 472-477, 2013.

Li, K., Jacob, D. J., Liao, H., Shen, L., Zhang, Q., and Bates, K. H.: Anthropogenic drivers of 2013-2017 trends in summer surface ozone in China, P Natl Acad Sci USA, 116, 422-427, 2019a.

Li, M. M., Song, Y., Huang, X., Li, J. F., Mao, Y., Zhu, T., Cai, X. H., and Liu, B.: Improving mesoscale modeling using satellite-derived land surface parameters in the Pearl River Delta region, China, J Geophys Res-Atmos, 119, 6325-6346, 2014.

Li, M. M., Wang, T. J., Shu, L., Qu, Y. W., Xie, M., Liu, J. N., Wu, H., and Kalsoom, U.: Rising surface ozone in China from 2013 to 2017: A response to the recent atmospheric warming or pollutant controls?, Atmos Environ, 246, 118130, doi: 10.1016/j.atmosenv.2020.118130, 2021a.

Li, M. M., Wang, T. J., Xie, M., Zhuang, B. L., Li, S., Han, Y., Song, Y., and Cheng, N. L.: Improved meteorology and ozone air quality simulations using MODIS land surface parameters in the Yangtze River Delta urban cluster, China, J Geophys Res-Atmos, 122, 3116-3140, 2017.

Li, M. M., Wang, T. J., Xie, M., Li, S., Zhuang, B. L., Huang, X., Chen, P. L., Zhao, M., and Liu, J. E.: Formation and Evolution Mechanisms for Two Extreme Haze Episodes in the Yangtze River Delta Region of China During Winter 2016, J Geophys Res-Atmos, 124, 3607-3623, 2019b.

627 Li, M. M., Wang, T. J., Xie, M., Li, S., Zhuang, B. L., Fu, Q. Y., Zhao, M., Wu, H.,
628 Liu, J., Saikawa, E., and Liao, K.: Drivers for the poor air quality conditions in
629 North China Plain during the COVID-19 outbreak, Atmos Environ, 246, 118103,
630 doi: 10.1016/j.atmosenv.2020.118103, 2021b.

631 Lin, Y. L., Farley, R. D., and Orville, H. D.: Bulk Parameterization of the Snow Field
632 in a Cloud Model, J Clim Appl Meteorol, 22, 1065−1092, 1983.

633 Liu, L., Bei, N. F., Hu, B., Wu, J. R., Liu, S. X., Li, X., Wang, R. N., Liu, Z. R., Shen,
634 Z. X., and Li, G. H.: Wintertime nitrate formation pathways in the north China
635 plain: Importance of N2O5 heterogeneous hydrolysis, Environ Pollut, 266,
636 115287, doi: 10.1016/j.envpol.2020.115287, 2020.

637 Liu, M. X., Huang, X., Song, Y., Tang, J., Cao, J. J., Zhang, X. Y., Zhang, Q., Wang,
638 S. X., Xu, T. T., Kang, L., Cai, X. H., Zhang, H. S., Yang, F. M., Wang, H. B.,
639 Yu, J. Z., Lau, A. K. H., He, L. Y., Huang, X. F., Duan, L., Ding, A. J., Xue, L.
640 K., Gao, J., Liu, B., and Zhu, T.: Ammonia emission control in China would
641 mitigate haze pollution and nitrogen deposition, but worsen acid rain, P Natl
642 Acad Sci USA, 116, 7760-7765, 2019.

643 Liu, X. H., Zhang, Y., Xing, J., Zhang, Q. A., Wang, K., Streets, D. G., Jang, C.,
644 Wang, W. X., and Hao, J. M.: Understanding of regional air pollution over China
645 using CMAQ, part II. Process analysis and sensitivity of ozone and particulate
646 matter to precursor emissions, Atmos Environ, 44, 3719-3727, 2010.

647 Liu, Y. M. and Wang, T.: Worsening urban ozone pollution in China from 2013 to
648 2017-Part 2: The effects of emission changes and implications for multi-pollutant
649 control, Atmos Chem Phys, 20, 6323-6337, 2020.

650 Luo, L., Zhu, R. G., Song, C. B., Peng, J. F., Guo, W., Liu, Y. H., Zheng, N. J., Xiao,
651 H. W., and Xiao, H. Y.: Changes in nitrate accumulation mechanisms as PM2.5
652 levels increase on the North China Plain: A perspective from the dual isotopic
653 compositions of nitrate, Chemosphere, 263, 127915, doi:
654 10.1016/j.chemosphere.2020.127915, 2021.

655 Meng, Z., Dabdub, D., and Seinfeld, J. H.: Chemical coupling between atmospheric
656 ozone and particulate matter, Science, 277, 116-119, 1997.

Nguyen, K. and Dabdub, D.: NOx and VOC control and its effects on the formation of aerosols, Aerosol Sci Tech, 36, 560-572, 2002.

Noh, Y., Cheon, W. G., Hong, S. Y., and Raasch, S.: Improvement of the K-profile model for the planetary boundary layer based on large eddy simulation data, Bound-Lay Meteorol, 107, 401−427, 2003.

Pathak, R. K., Wang, T., and Wu, W. S.: Nighttime enhancement of PM2.5 nitrate in ammonia-poor atmospheric conditions in Beijing and Shanghai: Plausible contributions of heterogeneous hydrolysis of N2O5 and HNO3 partitioning, Atmos Environ, 45, 1183-1191, 2011.

Pun, B. K. and Seigneur, C.: Sensitivity of particulate matter nitrate formation to precursor emissions in the California San Joaquin Valley, Environ Sci Technol, 35, 2979-2987, 2001.

Seinfeld, J. H. and Pandis, S. N.: Atmospheric chemistry and physics: from air pollution to climate change. 2nd Edition, John Wiley and Sons, Hoboken, NJ, 2006.

Shao, P. Y., Tian, H. Z., Sun, Y. J., Liu, H. J., Wu, B. B., Liu, S. H., Liu, X. Y., Wu, Y. M., Liang, W. Z., Wang, Y., Gao, J. J., Xue, Y. F., Bai, X. X., Liu, W., Lin, S. M., and Hu, G. Z.: Characterizing remarkable changes of severe haze events and chemical compositions in multi-size airborne particles (PM1, PM2.5 and PM10) from January 2013 to 2016-2017 winter in Beijing, China, Atmos Environ, 189, 133-144, 2018.

Shu, L., Wang, T. J., Xie, M., Li, M. M., Zhao, M., Zhang, M., and Zhao, X. Y.: Episode study of fine particle and ozone during the CAPUM-YRD over Yangtze River Delta of China: Characteristics and source attribution, Atmos Environ, 203, 87-101, 2019.

Silver, B., Reddington, C. L., Arnold, S. R., and Spracklen, D. V.: Substantial changes in air pollution across China during 2015-2017, Environ Res Lett, 14, 114012, 2018.

Smith, A., Lott, N., and Vose, R.: The Integrated Surface Database Recent Developments and Partnerships, B Am Meteorol Soc, 92, 704-708, 2011.

687 Sun, Y. L., Wang, Z. F., Dong, H. B., Yang, T., Li, J., Pan, X. L., Chen, P., and Jayne,
688 J. T.: Characterization of summer organic and inorganic aerosols in Beijing,
689 China with an Aerosol Chemical Speciation Monitor, Atmos Environ, 51, 250-
690 259, 2012.

691 Tsimpidi, A. P., Karydis, V. A., and Pandis, S. N.: Response of Fine Particulate
692 Matter to Emission Changes of Oxides of Nitrogen and-Anthropogenic Volatile
693 Organic Compounds in the Eastern United States, J Air Waste Manage, 58,
694 1463-1473, 2008.

695 Wang, G. H., Zhang, R. Y., Gomez, M. E., Yang, L. X., Zamora, M. L., Hu, M., Lin,
696 Y., Peng, J. F., Guo, S., Meng, J. J., Li, J. J., Cheng, C. L., Hu, T. F., Ren, Y. Q.,
697 Wang, Y. S., Gao, J., Cao, J. J., An, Z. S., Zhou, W. J., Li, G. H., Wang, J. Y.,
698 Tian, P. F., Marrero-Ortiz, W., Secrest, J., Du, Z. F., Zheng, J., Shang, D. J.,
699 Zeng, L. M., Shao, M., Wang, W. G., Huang, Y., Wang, Y., Zhu, Y. J., Li, Y. X.,
700 Hu, J. X., Pan, B., Cai, L., Cheng, Y. T., Ji, Y. M., Zhang, F., Rosenfeld, D., Liss,
701 P. S., Duce, R. A., Kolb, C. E., and Molina, M. J.: Persistent sulfate formation
702 from London Fog to Chinese haze, P Natl Acad Sci USA, 113, 13630-13635,
703 2016.

704 Wang, H. C., Lu, K. D., Chen, X. R., Zhu, Q. D., Chen, Q., Guo, S., Jiang, M. Q., Li,
705 X., Shang, D. J., Tan, Z. F., Wu, Y. S., Wu, Z. J., Zou, Q., Zheng, Y., Zeng, L.
706 M., Zhu, T., Hu, M., and Zhang, Y. H.: High N2O5 Concentrations Observed in
707 Urban Beijing: Implications of a Large Nitrate Formation Pathway, Environ Sci
708 Tech Let, 4, 416-420, 2017a.

709 Wang, J. D., Zhao, B., Wang, S. X., Yang, F. M., Xing, J., Morawska, L., Ding, A. J.,
710 Kulmala, M., Kerminen, V. M., Kujansuu, J., Wang, Z. F., Ding, D. A., Zhang,
711 X. Y., Wang, H. B., Tian, M., Petaja, T., Jiang, J. K., and Hao, J. M.: Particulate
712 matter pollution over China and the effects of control policies, Sci Total Environ,
713 584, 426-447, 2017b.

714 Wang, S. X., Xing, J., Zhao, B., Jang, C., and Hao, J. M.: Effectiveness of national air
715 pollution control policies on the air quality in metropolitan areas of China, J
716 Environ Sci, 26, 13-22, 2014.

717 Wang, X. F., Wang, W. X., Yang, L. X., Gao, X. M., Nie, W., Yu, Y. C., Xu, P. J.,
718 Zhou, Y., and Wang, Z.: The secondary formation of inorganic aerosols in the

719 droplet mode through heterogeneous aqueous reactions under haze conditions,
720 Atmos Environ, 63, 68-76, 2012.

721 Wang, Y., Zhang, Q. Q., He, K., Zhang, Q., and Chai, L.: Sulfate-nitrate-ammonium
722 aerosols over China: response to 2000-2015 emission changes of sulfur dioxide,
723 nitrogen oxides, and ammonia, Atmos Chem Phys, 13, 2635-2652, 2013.

724 Wang, Y. L., Song, W., Yang, W., Sun, X. C., Tong, Y. D., Wang, X. M., Liu, C. Q.,
725 Bai, Z. P., and Liu, X. Y.: Influences of Atmospheric Pollution on the
726 Contributions of Major Oxidation Pathways to PM2.5 Nitrate Formation in
727 Beijing, J Geophys Res-Atmos, 124, 4174-4185, 2019.

728 Wen, L., Xue, L. K., Wang, X. F., Xu, C. H., Chen, T. S., Yang, L. X., Wang, T.,
729 Zhang, Q. Z., and Wang, W. X.: Summertime fine particulate nitrate pollution in
730 the North China Plain: increasing trends, formation mechanisms and implications
731 for control policy, Atmos Chem Phys, 18, 11261-11275, 2018.

732 Wen, Z., Xu, W., Pan, X. Y., Han, M. J., Wang, C., Benedict, K., Tang, A. H., Collet,
733 J. L., and Liu, X. J.: Effects of reactive nitrogen gases on the aerosol formation
734 in Beijing from late autumn to early spring, Environ Res Lett, 16, 025005, doi:
735 10.1088/1748-9326/abd973, 2021.

736 Womack, C. C., McDuffie, E. E., Edwards, P. M., Bares, R., de Gouw, J. A.,
737 Docherty, K. S., Dube, W. P., Fibiger, D. L., Franchin, A., Gilman, J. B.,
738 Goldberger, L., Lee, B. H., Lin, J. C., Lone, R., Middlebrook, A. M., Millet, D.
739 B., Moravek, A., Murphy, J. G., Quinn, P. K., Riedel, T. P., Roberts, J. M.,
740 Thornton, J. A., Valin, L. C., Veres, P. R., Whitehill, A. R., Wild, R. J., Warneke,
741 C., Yuan, B., Baasandorj, M., and Brown, S. S.: An Odd Oxygen Framework for
742 Wintertime Ammonium Nitrate Aerosol Pollution in Urban Areas: NOx and
743 VOC Control as Mitigation Strategies, Geophys Res Lett, 46, 4971-4979, 2019.

744 Xie, M., Zhu, K. G., Wang, T. J., Yang, H. M., Zhuang, B. L., Li, S., Li, M. G., Zhu,
745 X. S., and Ouyang, Y.: Application of photochemical indicators to evaluate
746 ozone nonlinear chemistry and pollution control countermeasure in China,
747 Atmos Environ, 99, 466-473, 2014.

748 Xue, J., Yuan, Z. B., Lau, A. K. H., and Yu, J. Z.: Insights into factors affecting
749 nitrate in PM2.5 in a polluted high NOx environment through hourly

observations and size distribution measurements, J Geophys Res-Atmos, 119, 4888-4902, 2014.

Xue, J., Yuan, Z. B., Griffith, S. M., Yu, X., Lau, A. K. H., and Yu, J. Z.: Sulfate Formation Enhanced by a Cocktail of High NOx, SO2, Particulate Matter, and Droplet pH during Haze-Fog Events in Megacities in China: An Observation-Based Modeling Investigation, Environ Sci Technol, 50, 7325-7334, 2016.

Zaveri, R. A. and Peters, L. K.: A new lumped structure photochemical mechanism for large-scale applications, J Geophys Res-Atmos, 104, 30387-30415, 1999.

Zaveri, R. A., Easter, R. C., Fast, J. D., and Peters, L. K.: Model for Simulating Aerosol Interactions and Chemistry (MOSAIC), J Geophys Res-Atmos, 113, D13204, doi: 10.1029/2007jd008782, 2008.

Zhai, S. X., Jacob, D. J., Wang, X., Shen, L., Li, K., Zhang, Y. Z., Gui, K., Zhao, T. L., and Liao, H.: Fine particulate matter (PM2.5) trends in China, 2013-2018: separating contributions from anthropogenic emissions and meteorology, Atmos Chem Phys, 19, 11031-11041, 2019.

Zhang, W. Q., Tong, S. R., Ge, M. F., An, J. L., Shi, Z. B., Hou, S. Q., Xia, K. H., Qu, Y., Zhang, H. X., Chu, B. W., Sun, Y. L., and He, H.: Variations and sources of nitrous acid (HONO) during a severe pollution episode in Beijing in winter 2016, Sci Total Environ, 648, 253-262, 2019.

Zhang, Y. M., Wang, Y. Q., Zhang, X. Y., Shen, X. J., Sun, J. Y., Wu, L. Y., Zhang, Z. X., and Che, H. C.: Chemical Components, Variation, and Source Identification of PM1 during the Heavy Air Pollution Episodes in Beijing in December 2016, J Meteorol Res-Prc, 32, 1-13, 2018.

Zhao, M. F., Xiu, G. L., Qiao, T., Li, Y. L., and Yu, J. Z.: Characteristics of Haze Pollution Episodes and Analysis of a Typical Winter Haze Process in Shanghai, Aerosol Air Qual Res, 16, 1625-1637, 2016.

Zhao, P. S., Dong, F., He, D., Zhao, X. J., Zhang, X. L., Zhang, W. Z., Yao, Q., and Liu, H. Y.: Characteristics of concentrations and chemical compositions for PM2.5 in the region of Beijing, Tianjin, and Hebei, China, Atmos Chem Phys, 13, 4631-4644, 2013.

780 Zheng, B., Tong, D., Li, M., Liu, F., Hong, C. P., Geng, G. N., Li, H. Y., Li, X., Peng,
781 L. Q., Qi, J., Yan, L., Zhang, Y. X., Zhao, H. Y., Zheng, Y. X., He, K. B., and
782 Zhang, Q.: Trends in China's anthropogenic emissions since 2010 as the
783 consequence of clean air actions, Atmos Chem Phys, 18, 14095-14111, 2018.

784

785 **Table 1**. The emission scenarios in WRF-Chem numerical experiments

Simulation scenarios	Descriptions
B0	Base simulation under the 2016 emission conditions.
C_N (N=1/2/…/8)	Same as B0, but anthropogenic NO_x emissions are reduced by 10%, 20%...80%, respectively, relative to the usual levels in 2016.
$C_{S\text{-}N}$ (N=2/4/6/8)	Same as B0, but anthropogenic SO_2 emissions are reduced by 20%, 40%...80%, respectively, relative to the usual levels in 2016.
$C_{N\text{-}N}$ (N=2/4/6/8)	Same as B0, but anthropogenic NH_3 emissions are reduced by 20%, 40%...80%, respectively, relative to the usual levels in 2016.
$C_{V\text{-}N}$ (N=2/4/6/8)	Same as B0, but anthropogenic VOC_s emissions are reduced by 20%, 40%...80%, respectively, relative to the usual levels in 2016.
N0	Same as B0, but only consider the NO_2+OH gas-phase oxidation pathway for the production of nitrate aerosol.
E1	Same as B0, but anthropogenic NO_x emissions are replaced using the MEIC inventory in 2012.

786

787 **Table 2**. Statistical evaluations of the model meteorological performance

Variable	Obs	Sim	R [a]	MB [a]	NMB [a]	ME [a]	RMSE [a]
Period I (15 August to 16 September)							
Temperature (℃)	24.04	23.91	0.89	−0.13	−0.55%	1.98	2.63
Humidity (%)	70.89	66.88	0.78	−4.01	−5.65%	11.07	14.67
Wind speed (m s^{-1})	2.46	3.04	0.50	0.58	23.72%	1.38	1.83
Period II (24 November to 26 December)							
Temperature (℃)	3.43	3.40	0.94	−0.03	−0.80%	2.18	2.83
Humidity (%)	69.85	65.27	0.63	−4.58	−6.56%	13.51	17.88
Wind speed (m s^{-1})	2.61	3.66	0.55	1.06	40.64%	1.70	2.23

788 [a] R: correlation efficient; MB: mean bias; NMB: normalized mean bias; ME: mean
789 error; RMSE: root mean square error.

790

791

792 **Table 3**. Statistical evaluations of the model chemical performance

Variable	Obs	Sim	MB	NMB	Obs	Sim	MB	NMB
		Period I				Period II		
$PM_{2.5}$	36.88	33.22	−3.66	−9.92%	91.59	64.28	−27.31	−29.82%
SO_2	17.65	16.51	−1.14	−6.46%	41.45	29.80	−11.65	−28.11%
NO_2	28.53	33.23	4.70	16.47%	53.01	54.28	1.27	2.40%
Daily-maximum O_3	237.45	255.77	18.32	7.72%	125.62	86.61	−39.01	−31.05%

793

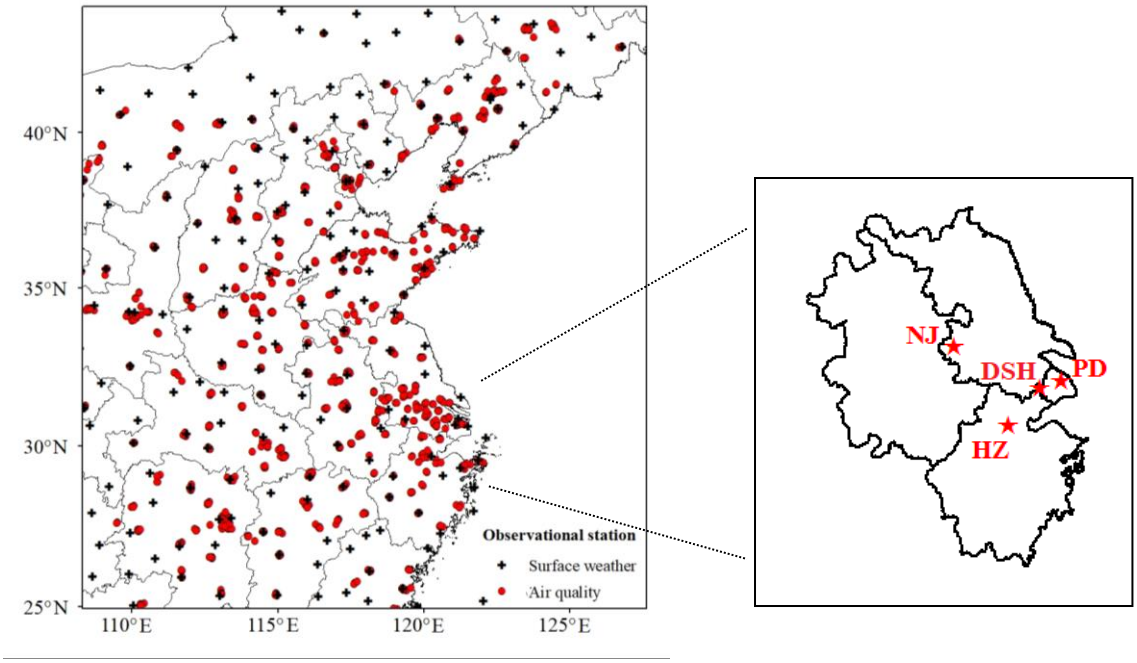

794 **Fig. 1**. WRF-Chem domain configuration and observational stations. Black crosses:
795 surface weather stations; Red dots: CNEMC routine air quality monitoring stations;
796 Red stars: surface supersites in YRD.

797

798

799

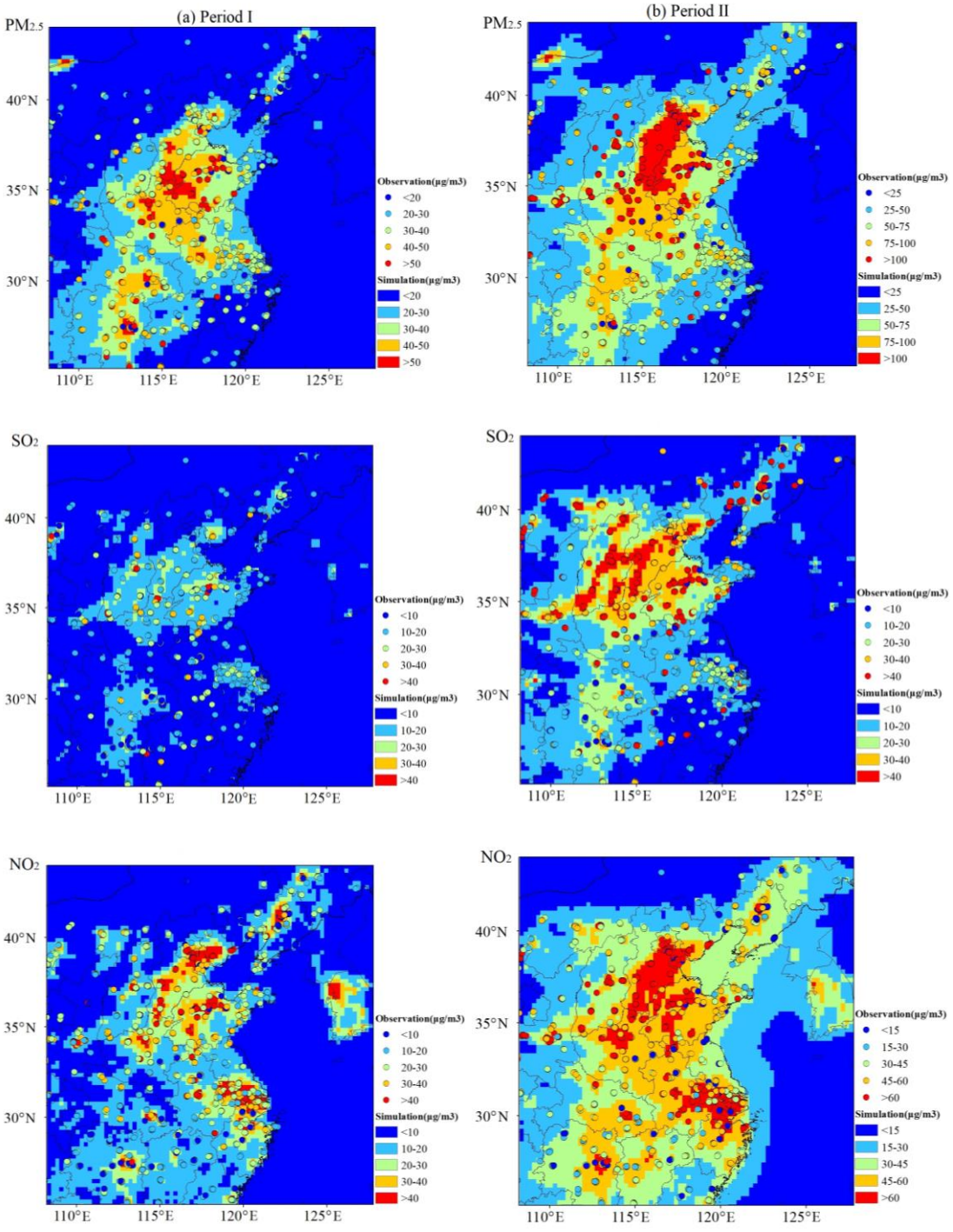

800 **Fig. 2**. Spatial patterns of the surface average $PM_{2.5}$, NO_2, SO_2 and daily-maximum
801 O_3 concentrations in Period I (left panels) and Period II (right panels) from the WRF-
802 Chem modeling (shaded contours) and routine air quality observations (dots).

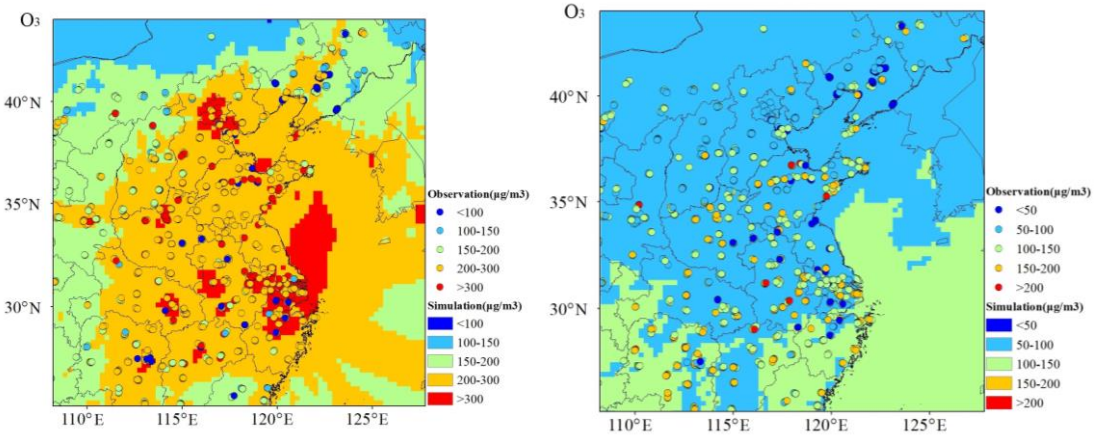

803

804 **Fig. 2**. Continued.

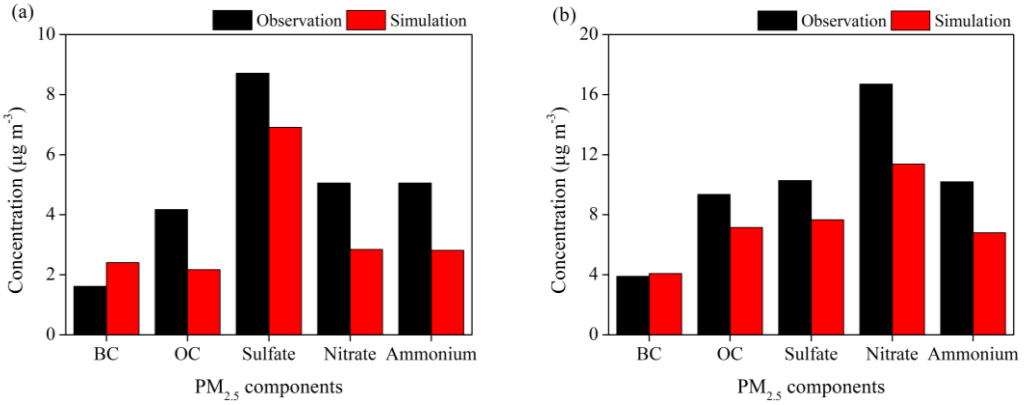

805

806 **Fig. 3**. Comparisons of surface $PM_{2.5}$ components from WRF-Chem simulations and
807 observations in Period I (a) and Period II (b) at the four supersites in YRD.

808

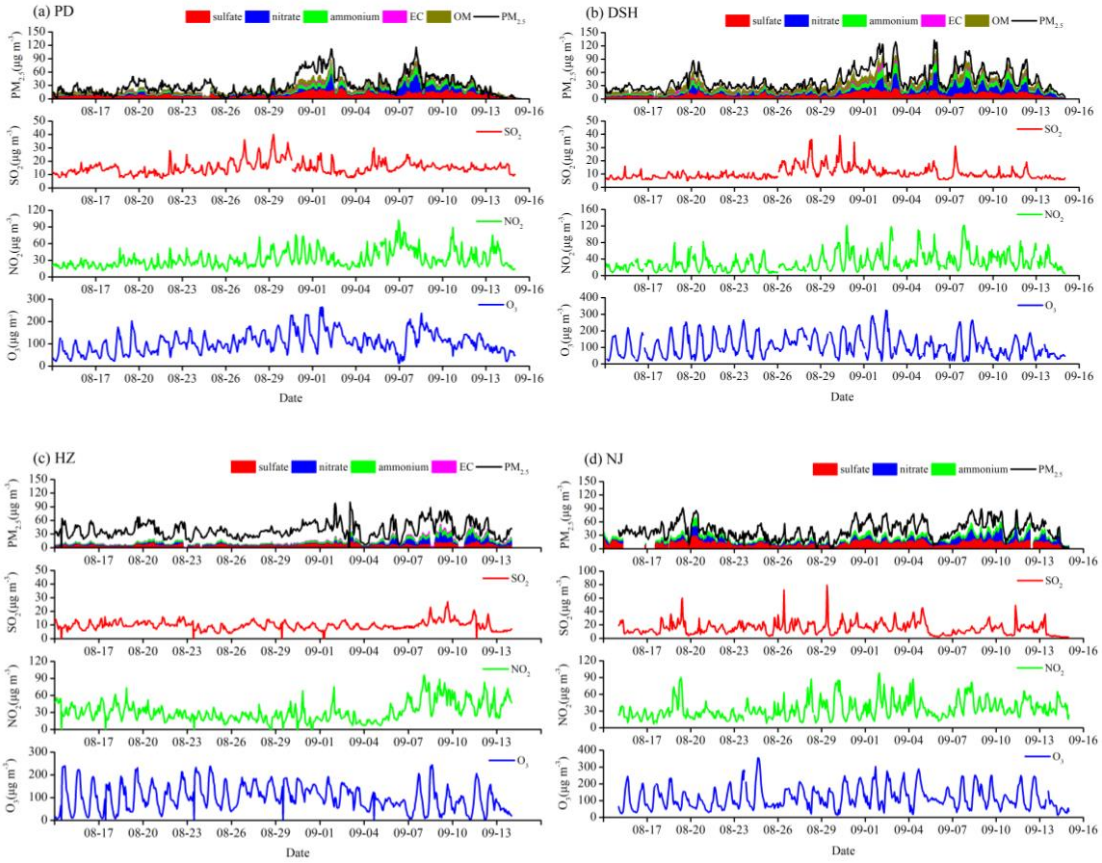

Fig. 4. Observed aerosol composition and gaseous pollutants concentrations at the four supersites during Period I.

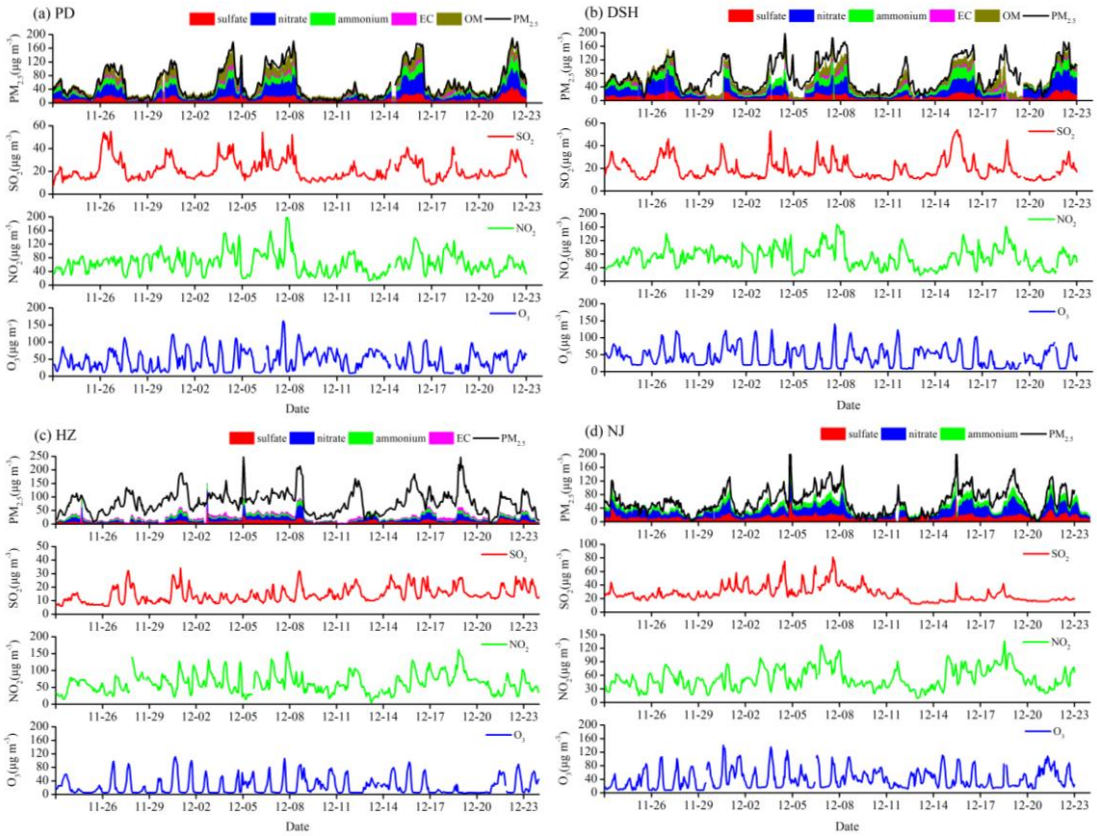

Fig. 5. Same as Fig. 4, but for Period II.

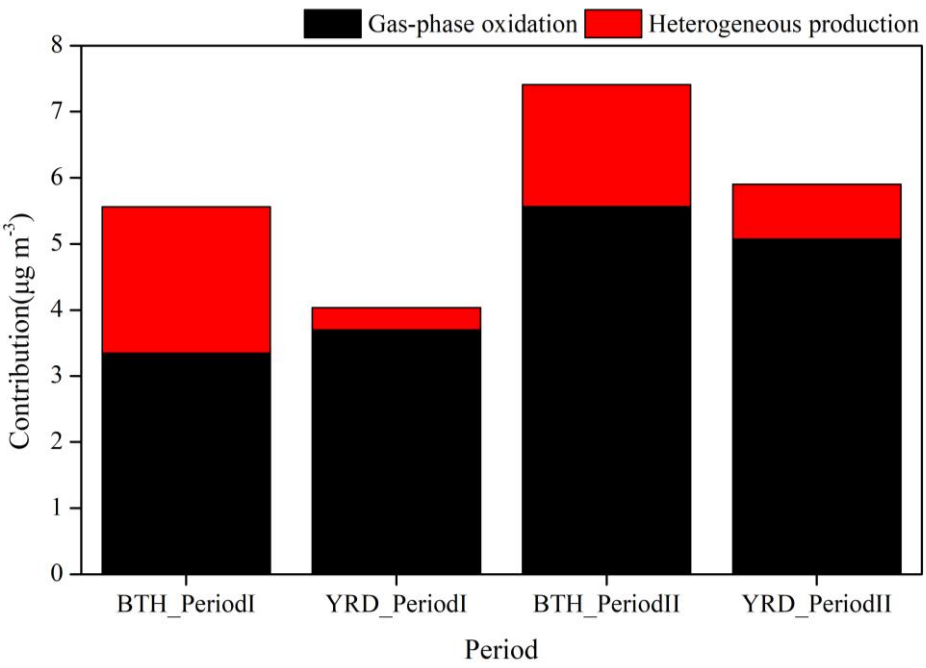

817

818 **Fig. 6**. Contributions of gas-phase oxidation and heterogeneous production to the
819 surface nitrate concentrations for the BTH and YRD regions in two seasons.

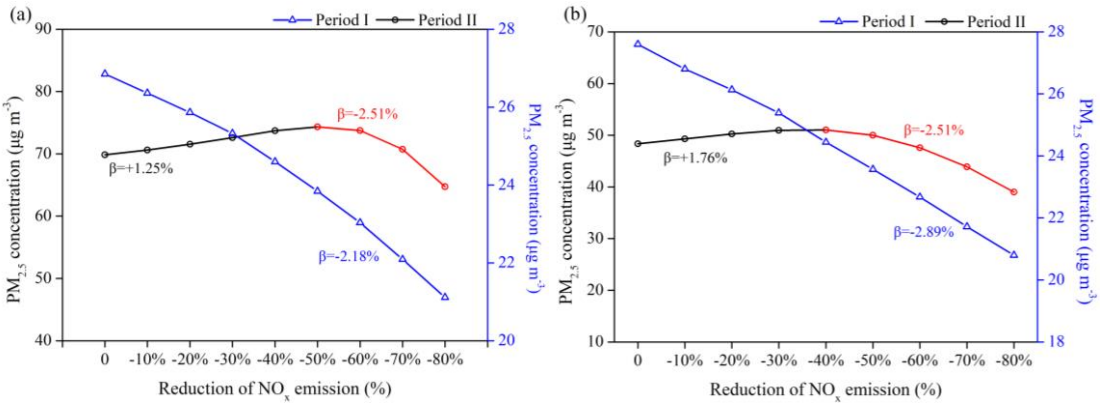

820

821 **Fig. 7**. Responses of surface $PM_{2.5}$ concentrations to the NO_x emission reduction
822 scenarios in (a) BTH and (b) YRD. The calculated NO_x emission control efficiency (β)
823 is also marked in the figure.

824

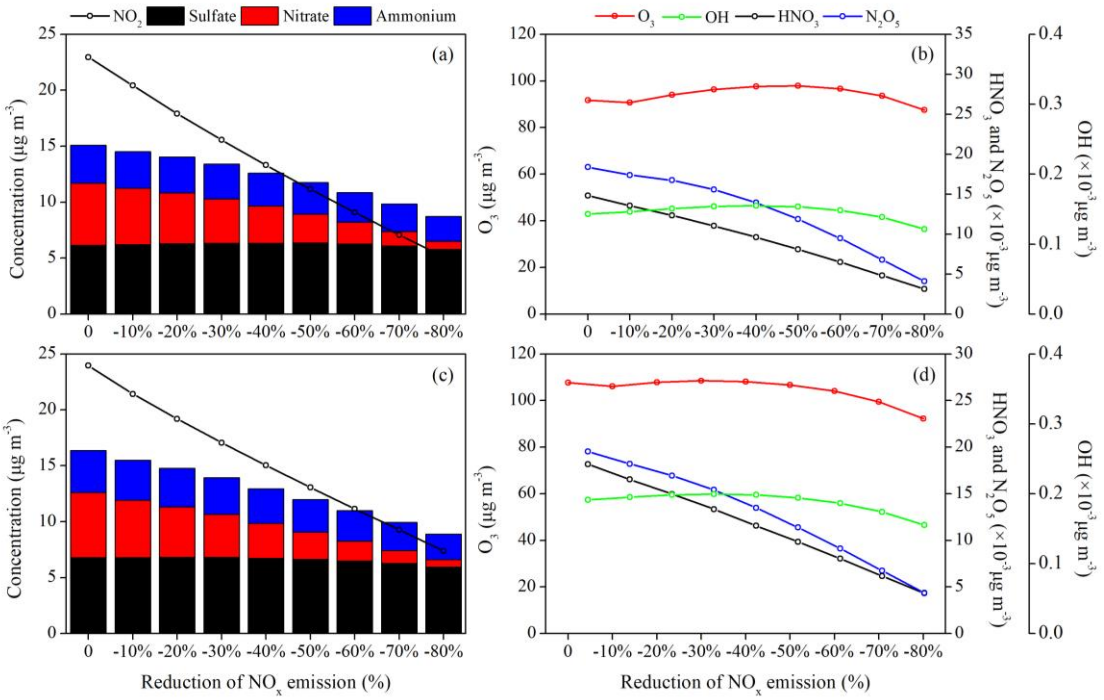

Fig. 8. Responses of the surface concentrations of SIA components and key atmospheric trace gases (NO_2, O_3, OH, HNO_3 and NO_3) to the NO_x emission reduction scenarios in (a, b) BTH and (c, d) YRD during Period I.

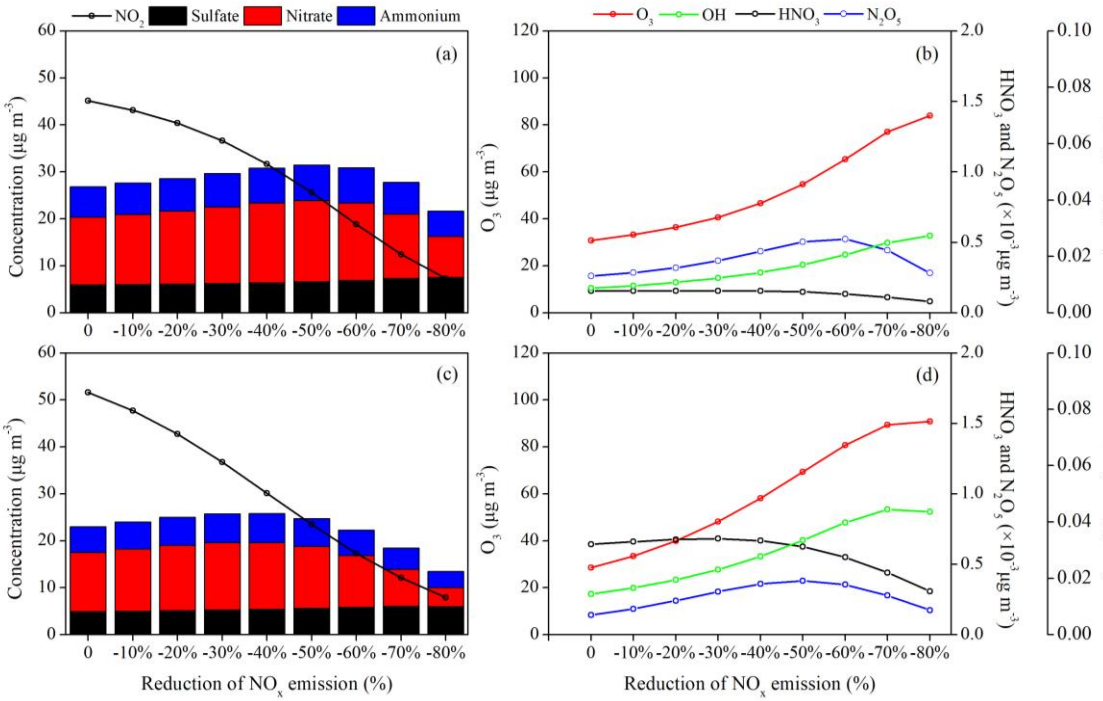

Fig. 9. Same as Fig. 8, but for Period II.

832

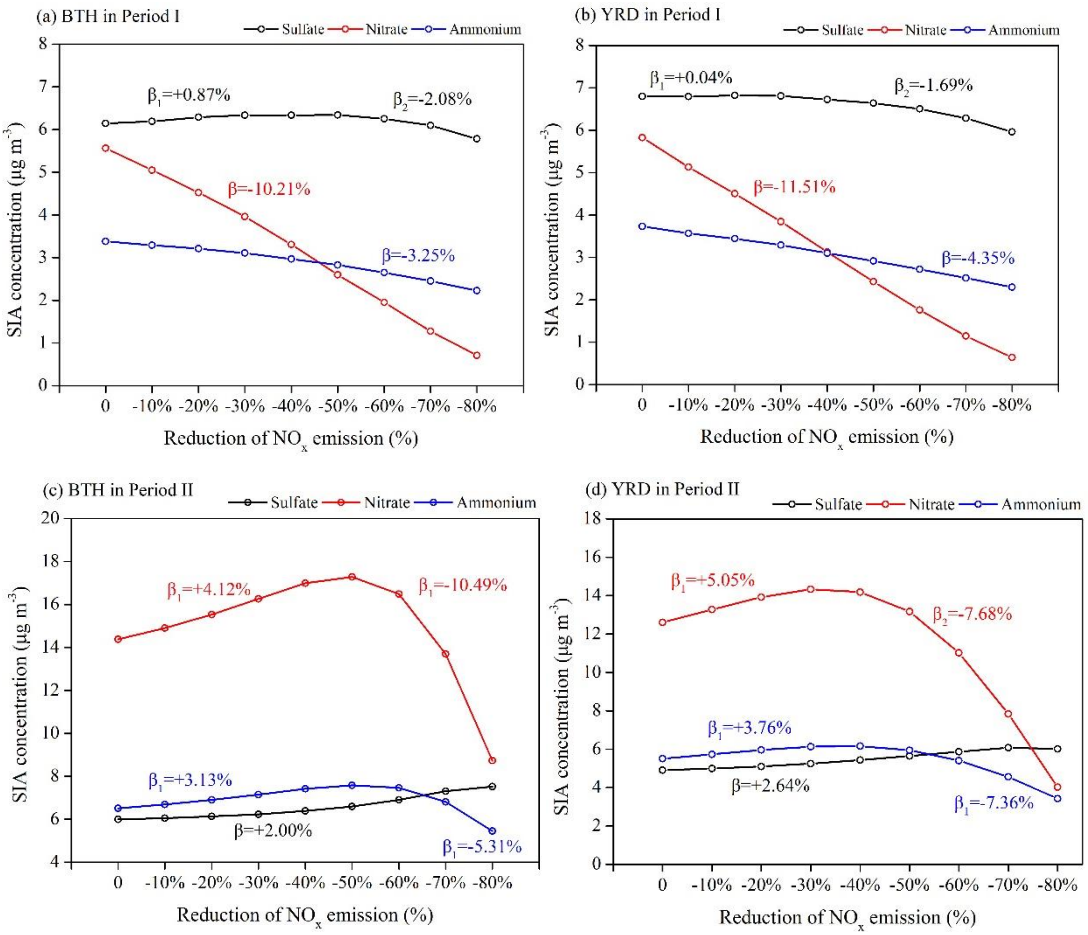

833

834 **Fig. 10**. Responses of the surface concentrations of SIA components to the NO_x
835 emission reduction scenarios and their emission control efficiencies in (a, b) Period I
836 and (c, d) Period II.

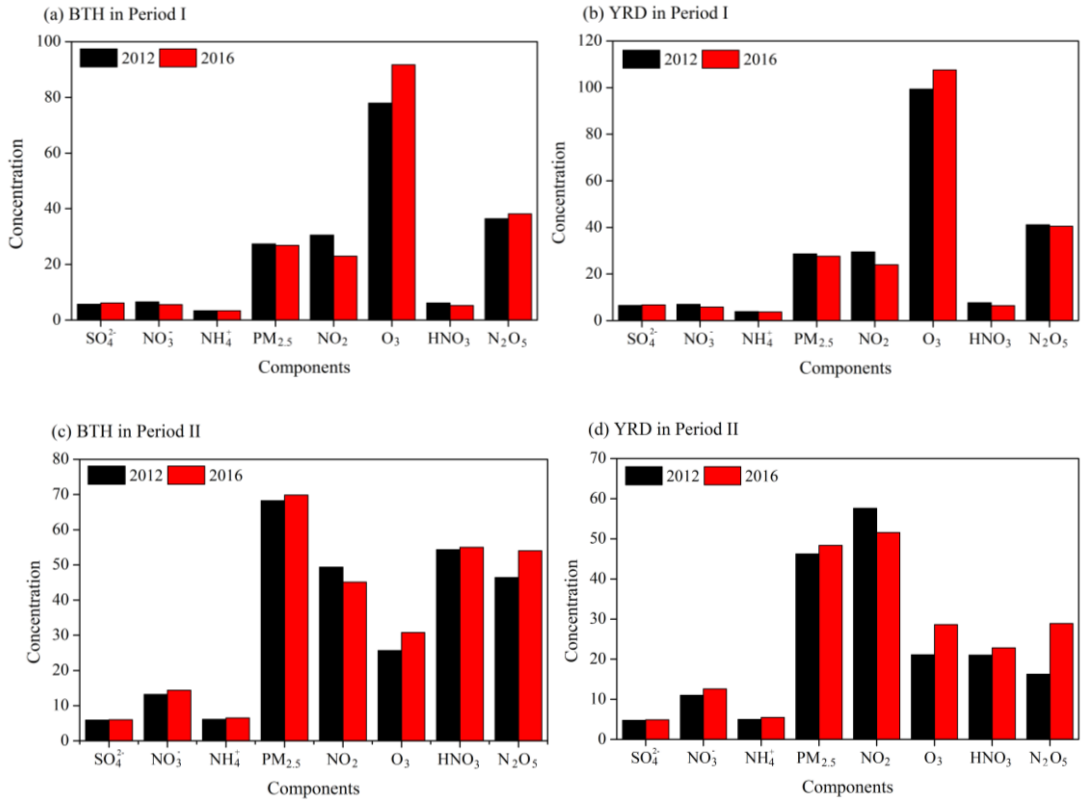

Fig. 11. Changes in the concentrations of surface $PM_{2.5}$, SIA components and key atmospheric trace (NO_2, O_3, HNO_3 and N_2O_5) due to the 2012–2016 NO_x emission reductions in China estimated as the differences between the base simulation and E1 scenario. The units are ppt for HNO_3 and N_2O_5, and μg m^{-3} for other chemical species.

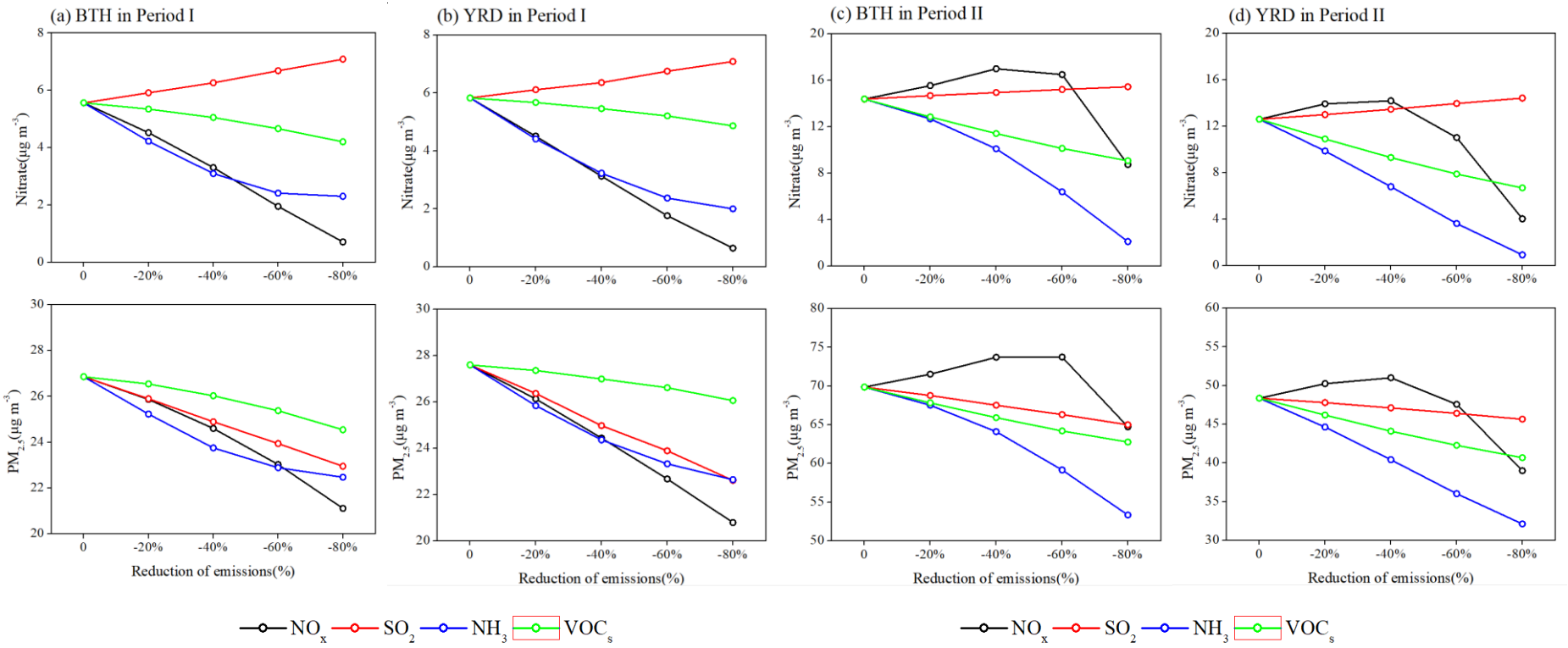

843

844

845 **Fig. 12**. Responses of the surface nitrate (upper panels) and $PM_{2.5}$ (bottom panels) concentrations to the emission reduction scenarios of NO_x,

846 SO_2, NH_3 and VOC_s during Period I (a, b) and Period II (c, d).